Exchange frequencies and magnetic ground state of Wigner crystal in anisotropic two-dimensional electron systems

Chenggang Zhou*
Department of Electrical Engineering, Princeton University, Princeton, New Jersey 08544, USA

R. N. Bhatt
Department of Electrical Engineering and Princeton Institute for the Science and Technology of Materials, Princeton University, Princeton, New Jersey 08544, USA

(Received 25 August 2006; published 20 November 2006)

We investigate the effect of mass anisotropy on the magnetic structure of the Wigner crystal of low-density electron systems in two dimensions at $T=0$. The multiparticle exchange frequencies are calculated with effective mass anisotropy, with and without concomitant lattice distortions. Numerical diagonalization of small lattice sizes with two-, three-, and four-spin exchange terms shows a transition from a ferromagnetic to an antiferromagnetic ground state with increasing mass anisotropy. We map out this transition at various electron densities.

DOI: 10.1103/PhysRevB.74.205325 PACS number(s): 73.20.Qt, 71.45.Gm, 71.70.Gm

I. INTRODUCTION

A system of interacting electrons at low densities, when the Coulomb interaction dominates the kinetic energy, is predicted to form a Wigner crystalline phase.[1] In two dimensions, quantum Monte Carlo simulations have predicted the critical density of crystallization to be given by $r_s=37\pm5$,[2] where the dimensionless parameter r_s is related to the electron density n_s by $r_s^{-1}=a_B(\pi n_s)^{1/2}$, with a_B being the Bohr radius. In the Wigner-crystal phase, multiparticle exchange processes are believed to control the spin degrees of freedom, and determine the magnetic phase of the electron system at low temperatures. The effective Hamiltonian in spin space for multiparticle exchange processes has the form proposed by Thouless;[3]

$$H=-\sum_P \mathrm{sgn}(P)J_P\hat{P}, \tag{1}$$

where the sum is over all possible permutations P involving any number of electrons, J_p is the exchange frequency, and $\hat{P}$ is the permutation operator, which acts on the spin-wave function. For instance, two-spin exchange[4] can be written as

$$\hat{P}_{ij}=\tfrac{1}{2}(1+\sigma_i\cdot\sigma_j), \tag{2}$$

where σ_i and σ_j are the Pauli matrices for the two electrons (labeled i and j) being exchanged. Conventionally, J_P is positive while the sign of each term is the sign of its permutation operator. For ring exchanges, $\mathrm{sgn}(P)=-1$ for exchanges involving an even number of spins, and +1 for those involving an odd number of spins. The three-spin exchange operator $\hat{P}_{ijk}$ can also be reduced to a sum of such Heisenberg-type two-spin couplings. However, the exchange operators of more than three spins contain the term $(\sigma_i\cdot\sigma_j)(\sigma_k\cdot\sigma_l)$, which cannot be omitted in some physical systems.

The Thouless Hamiltonian Eq. (1) has been used by many authors to study strongly interacting systems, such as ^{3}He in solid phase[5–7] and on graphite surface,[8] high-T_c superconductors,[9–11] two-dimensional (2D) electron Wigner crystal,[12] and spin ladders.[13–15] In all cases, it is believed that ring-exchange operators involving a few particles are important. Even with this assumption, this Hamiltonian contains enough complexity leading to several distinct phases. For example, a solid ^{3}He film on graphite exhibits a transition from a ferromagnetic phase to a nonmagnetic gapped spin-liquid phase, found by exact diagonalization of small clusters;[8] and spin excitations in La_2CuO_4 are described by self-consistent spin-wave theory with four-spin ring exchanges.[10]

In the case of the isotropic 2D electron Wigner crystal on a triangular lattice, not only two- and three-spin exchanges, but also four-, five-, and six-spin exchanges are competing with each other, giving rise to a complex phase diagram, which has ferromagnetic, spin liquid, and frustrated antiferromagnetic phases[16,17] among various possibilities. The exchange frequencies of multiparticle ring exchanges were first evaluated by Roger,[5] with a multidimensional WKB approximation. Recently, Voelker and Chakravarty[12] did a calculation for a 2D electron Wigner solid with instanton approximation, and these exchange frequencies have also been calculated with quantum Monte Carlo simulations by Bernu *et al.*[16] Compared with the numerically exact results, the WKB approximation is not quite accurate at small r_s; but it is increasingly accurate for large r_s, which is relevant for our study of electron Wigner crystals in low densities. In this large r_s (low density) limit, previous calculations show that the three-spin exchange frequency is the largest, and thus the three-spin exchange is the dominant term in the Hamiltonian giving rise to a ferromagnetic ground state.

The above conclusion is based on the assumption that the electron system is isotropic. In this paper, we consider the Wigner crystal of an anisotropic 2D electron system. Effective mass anisotropy is present in several semiconductor systems, such as Si or AlAs(110) surface and 2D electron systems in organic semiconductor crystals with low symmetry. Wan and Bhatt[18] suggested that in such anisotropic 2D electron systems, the mass anisotropy leads to an oblique Wigner lattice due to the competition between electrostatic energy

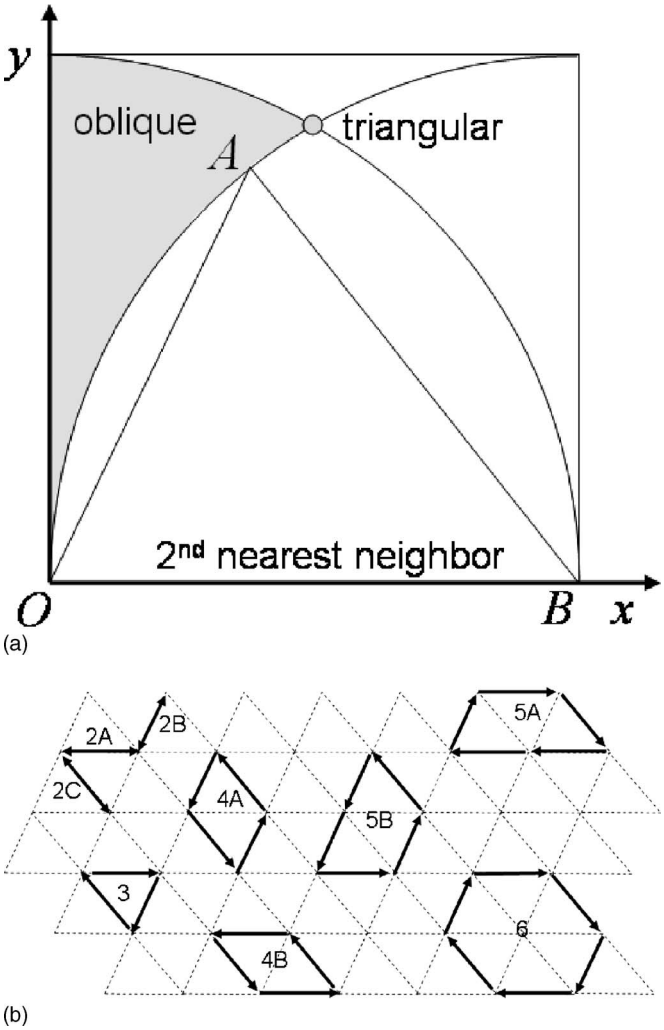

FIG. 1. (a) Parametrization of the oblique unit cell of the Wigner crystal following Ref. 18. The second-nearest neighbor is along the x axis and the oblique lattice is uniquely specified by a point in the shaded region. (b) Various ring-exchange processes considered in this paper. Different orientations of the two-, four-, and five-particle exchanges (which are identical for the triangular Wigner crystal) have different exchange frequencies in the presence of anisotropy.

and zero-point vibrational energy of the lattice. For a 2D electron Wigner crystal on Si(110) surface, the shape of the oblique unit cell is specified by two lattice vectors $\overline{OA}$ and $\overline{OB}$ in Fig. 1(a), where the longer second-neighbor distance $\overline{OB}$ is shown aligned in the x direction. The stable configuration was found to satisfy $|OA| < |OB| = |AB|$, and the position of point A is a function of the electron density.[18] Thus in general, we have two types of anisotropy, mass anisotropy, and lattice anisotropy; both of them affect the exchange frequencies.

Here, we address the question of what effect anisotropy has on the exchange frequencies and the magnetic ground state. The types of ring-exchange processes that we have studied are illustrated in Fig. 1(b). With mass and lattice anisotropy, there are three different two-particle exchange processes in three different directions. Both four- and five-particle exchanges split into two processes with different exchange frequencies. They do not split into three different processes because the stable oblique lattice are made of isosceles triangles. However, the exchange frequencies of three-particle and six-particle exchanges are independent of their orientations due to their symmetry.

In Sec. II, we present the calculation of exchange frequencies, and in Sec. III we present the calculation of the ground state of a 16-site cluster with anisotropic exchange frequencies. Our results show that with increasing mass anisotropy, the most important exchange process changes from three-particle exchange to the nearest-neighbor two-particle exchange. As a consequence, there is a phase transition from a ferromagnetic to an antiferromagnetic ground state as a function of mass anisotropy.[19]

II. EXCHANGE FREQUENCIES FOR MULTIPARTICLE EXCHANGES

A. Theoretical background

We have followed the formalism described in detail in Ref. 12 to compute the exchange frequencies, which is based on the WKB approach and uses the instanton approximation. In the instanton approximation, exchange processes are considered to be fast processes localized on the imaginary time axis. Their time scale $\delta\tau$ is of the order of the inverse phonon frequency. They are also considered to be rare events, i.e., the average time interval between two successive exchange processes ΔT is much larger than $\delta\tau$. Under this assumption, one considers the propagator on a time scale T that satisfies $\delta\tau \ll T \ll \Delta T$. Denoting the positions of all electrons sitting on the equilibrium state by the collective coordinate $\mathbf{R} = (\mathbf{r}_1, \ldots, \mathbf{r}_n)$, and the displacement form the equilibrium sites by $\mathbf{u} = (\mathbf{u}_1, \ldots, \mathbf{u}_n)$, we define $G(\mathbf{R}+\mathbf{u}_1, \mathbf{R}+\mathbf{u}_2, T)$ as the Green's function for the propagation of the lattice from the configuration $\mathbf{R}+\mathbf{u}_1$ at time $t=0$ to the configuration $\mathbf{R}+\mathbf{u}_2$ at time $t=T$. These Green's functions only represent the propagation of distinguishable spin-0 particles. The complete many-body electron propagators are constructed by appending spin indices to G followed by antisymmetrization. The exchange frequency J_p for a permutation P is derived in Ref. 12, which reads

$$J_P = \frac{G(\mathbf{R}+\mathbf{u}_1, P\mathbf{R}+P\mathbf{u}_2, T)}{TG(\mathbf{R}+\mathbf{u}_1, \mathbf{R}+\mathbf{u}_2, T)}, \tag{3}$$

i.e., the ratio of the Green's function for the evolution to a nearby permuted configuration to that for the same configuration without the permutation (exchange).

In the instanton approximation, this ratio can be evaluated to be

$$J_P = \sqrt{\frac{S_P}{2\pi\hbar m^\star}} \left(\frac{\det[-m^\star\partial_\tau^2 + V_{\mu\nu}(0)]}{\det'[-m^\star\partial_\tau^2 + V_{\mu\nu}(\tau)]} \right)^{1/2} e^{-S_P/\hbar}, \tag{4}$$

where S_p is the action corresponding to the classical exchange path of least action, and the determinants in the prefactor come from performing the Gaussian integral accounting for the quadratic quantum fluctuations around the classical path. The path with exchange has a zero-mode fluc-

tuation corresponding to the shift of the exchange event in the imaginary time, which is a Goldstone mode in this formalism. The prime in the determinant indicates that this zero mode is excluded. A detailed derivation[12] shows that this zero mode is taken care of by the prefactor $\sqrt{\frac{S_P}{2\pi\hbar m^\star}}$.

With anisotropy in the system, Eq. (4) is still valid after replacing $m^\star$ with $m_x^\star$ and $m_y^\star$ appropriately, e.g., the kinetic energy is expressed as

$$E_k = \frac{1}{2}\sum_n m_x^\star \left(\frac{dx^{(n)}}{d\tau}\right)^2 + m_y^\star \left(\frac{dy^{(n)}}{d\tau}\right)^2. \tag{5}$$

For convenience we define an average effective mass $m^\star = \sqrt{m_x^\star m_y^\star}$, which enters the expression for r_s and energy unit Ry. In our calculations, we use $m_x^\star = 0.190$ and $m_y^\star = 0.585$, which are the values for the Si(110) surface,[20] so that the ratio between the two effective masses is approximately 1:3. Wan and Bhatt[18] showed that such an anisotropy is large enough to tilt the Wigner crystal after considering the zero-point energy of lattice vibration. We use the lattice structure calculated by Wan and Bhatt[18] with $r_s = 100$ as an example of lattice distortion in our calculations. In this case, if we adopt the parametrization illustrated in Fig. 1(a), and measure distances in units of the second-nearest neighbor, the nearest neighbor is at (0.405, 0.806). For comparison, the triangular lattice corresponds to a point at (0.5, 0.866). We use a dielectric constant of silicon $\epsilon = 11.7$ in our calculations.

Following Ref. 12, we find the classical path by dividing the path into 16 segments and searching for the least action by the quasi-Newton algorithm. The long-range Coulomb potential is handled by an Ewald summation; its first- and second-order derivatives are calculated by taking the derivatives of the Ewald summation term by term. During the calculation, we have allowed 37–144 electrons in a Wigner crystal to move around. The remaining electrons are fixed on their equilibrium lattice sites so that they only contribute to the potential energy of the movable electrons. We have arranged the movable electrons in triangular-, hexagonal-, or parallelogram-shaped clusters to look for the effects of boundary conditions. For each cyclic exchange process, a number of electrons near the center exchange their positions cyclically. Movable electrons are added layer by layer surrounding the permuting electrons in order to extrapolate to the thermodynamic limit. Our results for the exchange frequencies from clusters of different shapes are in good agreement with each other, therefore the shape of the cluster does not bring a noticeable error. The prefactor is calculated by approximating $V_{\mu\nu}(\tau)$ in Eq. (4) with a piecewise constant potential, and keeping only the quadratic order. The zero mode becomes a finite eigenvalue due to this approximation. An iterative search for the shifted zero mode is necessary. Each search requires calculating the matrix elements of a very large matrix and diagonalizing it, so it takes much more CPU time than finding the classical trajectory. We have found that the shifted zero mode is always positive and usually one order of magnitude smaller than the next eigenvalue.

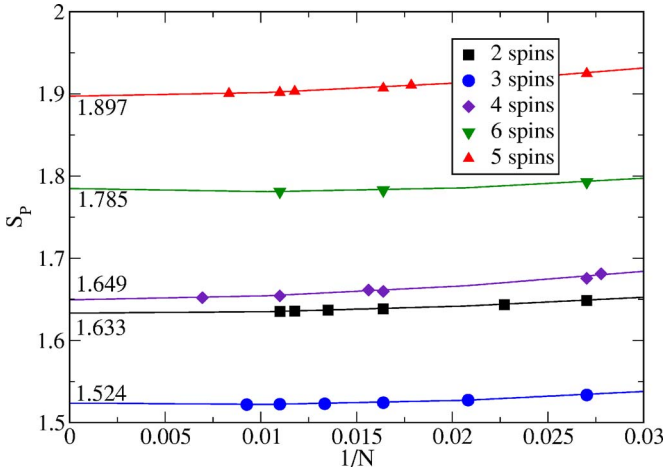

FIG. 2. (Color online) Effective actions S_P of five different ring-exchange processes for the isotropic lattice corresponding to 2, 3, 4, 5, and 6 spins. The curves are fits of the form $\alpha_0 + \frac{\alpha_1}{N} + \frac{\alpha_2}{N^2}$; the extrapolated value of thermodynamic limits (α_0) are marked in the figure.

B. Isotropic case

The calculation for the isotropic Wigner crystal was performed to compare our results with those of Ref. 12. For numerical calculations, Eq. (4) is simplified to[12]

$$\frac{J_P}{Ry} = A_P r_s^{-5/4} \sqrt{\frac{S_P}{2\pi}} \exp\{-\sqrt{r_s} S_P\}, \tag{6}$$

where S_P is the effective action, A_P is a prefactor from the ratio of determinants in Eq. (4), and Ry is the effective Rydberg constant. Our results for S_P and A_P are shown in Figs. 2 and 3, respectively. The effective action S_P slightly decreases with increasing cluster size N (the number of electrons allowed to move), which had not been reported previously. The extrapolated values are slightly below the values

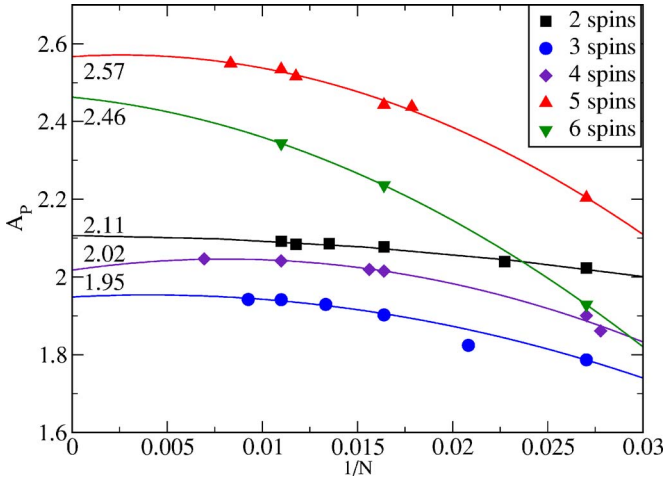

FIG. 3. (Color online) Numerical prefactors A_P for the five different ring-exchange processes. The curves are fits of the form $\alpha_0 + \frac{\alpha_1}{N} + \frac{\alpha_2}{N^2}$; the extrapolated value of thermodynamic limits are marked in the figure.

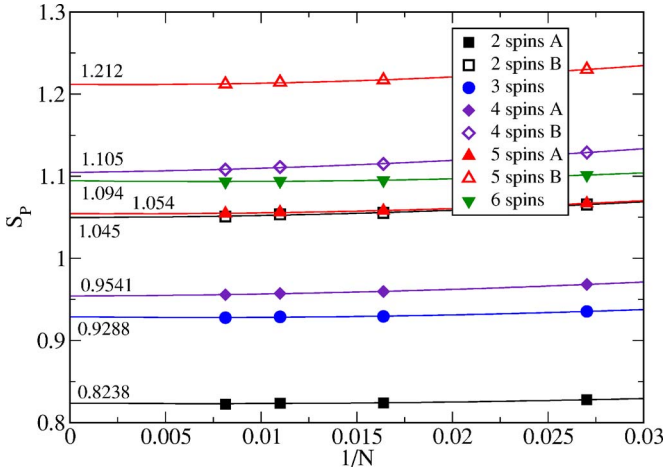

FIG. 4. (Color online) Effective actions S_P of different exchange processes for the Wigner crystal with mass anisotropy but *without* lattice distortion. Orientation A is along the x axis. The curves are fits of the form $\alpha_0+\frac{\alpha_1}{N}+\frac{\alpha_2}{N^2}$; the extrapolated value of thermodynamic limits are marked in the figure.

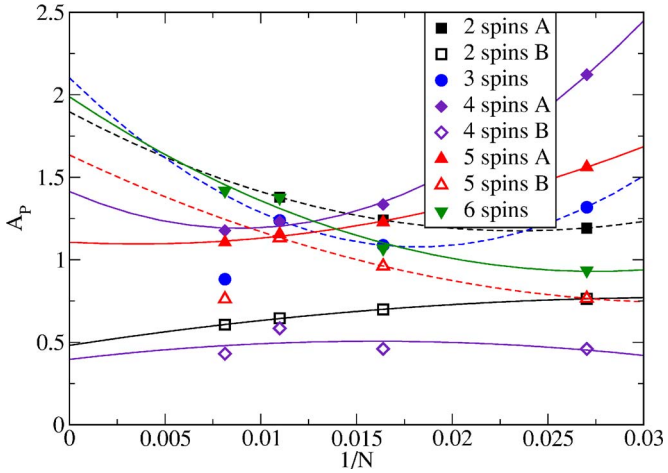

FIG. 5. (Color online) Numerical prefactors A_P of different exchange processes for the Wigner crystal with mass anisotropy *without* lattice distortion. Orientation A is along the x axis. The curves are fits of the form $\alpha_0+\frac{\alpha_1}{N}+\frac{\alpha_2}{N^2}$. The solid curves are fitted with four data points, while the dashed curves are fitted without the last data point $N=123$.

in Ref. 12; however, the differences are less than 1%. In the case of the prefactor A_P, the extrapolated values are about 10–15 % lower than those in Ref. 12; nevertheless, the trends of the extrapolations are the same. The differences may be attributed to minor differences in the method of calculation. It is easy to see that the ratio between these prefactors are of order unity. Since J_P depends on S_P and r_s exponentially, minor differences in A_P will not alter the qualitative behavior in the low densities ($r_s \sim 100$).

C. Anisotropic system

For each type of exchange process, since the data points calculated with different numbers of movable electrons almost fall on the same curve in the isotropic case, for the anisotropic Wigner crystal, we consider four sizes of clusters from 37 electrons to 123 electrons arranged in a hexagonal shape. These calculations are sufficient to demonstrate the difference from the isotropic case. The effective actions of exchange processes with anisotropic effective masses are generally smaller than the isotropic case because the average effective mass is smaller.

We introduce the anisotropy in two steps, to see first the effect of pure mass anisotropy on exchange frequencies with no lattice distortion, and secondly, the effect of both effective mass anisotropy and lattice distortion, with the lattice distortion calculated in Ref. 18 as our input. Figure 4 shows the effective actions of Wigner crystal with mass anisotropy but not lattice anisotropy, i.e., the exchange processes start from and end on a triangular lattice, while mass anisotropy is included in the kinetic energy. Due to the anisotropy, two-particle exchange splits into two different processes depending on the relative orientation of those two electrons exchanging their positions (x direction is parallel to the direction of the nearest neighbor of the triangular lattice), as well as four- and five-particle exchanges. We see that the smallest S_P belongs to the two-particle exchange A, which is along the x direction (see Fig. 1; 2B and 2C are equivalent if the lattice is triangular). A large gap between the smallest S_P and the second least S_P, which is given by the three-particle exchange process, is also seen in Fig. 4.

Figure 5 shows the corresponding numerical prefactor for each exchange process in Fig. 4. The curves obtained by fitting do not appear regularly monotonic as in the isotropic case. For two-spin exchange type A, three-spin exchange, and five-spin exchange type B, the last data points at $N=123$ obviously deviate from the fitting curve consistent with the other three data points of smaller cluster sizes, therefore $N=123$ is excluded from the curve fitting in these three cases. These large deviations could indicate a numerical instability for large cluster sizes in the algorithm for calculating A_P. The overall error of the calculated A_P is estimated to be about 10% as will be discussed in the context of Fig. 7. We can only reliably conclude that these prefactors are of order unity. Fortunately, in the low-density regime that we are interested in, differences of order unity between A_Ps will be dominated by the exponential dependence on r_s.

Figures 6 and 7 show our results with both mass anisotropy and lattice distortion for the oblique lattice determined for $r_s=100$.[18] The effective actions shown in Fig. 6 appear in a narrower range than the previous results calculated without lattice anisotropy. The extrapolated actions of nearest-neighbor and second-nearest-neighbor exchanges seem to coincide with each other, both being the smallest effective action. Above them is the three-spin exchange. The two-particle exchange of type C appears to be at the top of this figure. With lattice anisotropy, the effective actions also show a stronger size dependence than those in Figs. 2 and 4.

Figure 7 shows the numerical prefactor A_P corresponding to exchange processes in Fig. 6. Similar to Fig. 5, A_P calculated for several exchange processes with $N=123$ are not consistent with those from three smaller clusters. As in Fig. 5, these data points at $N=123$ are excluded from the curve

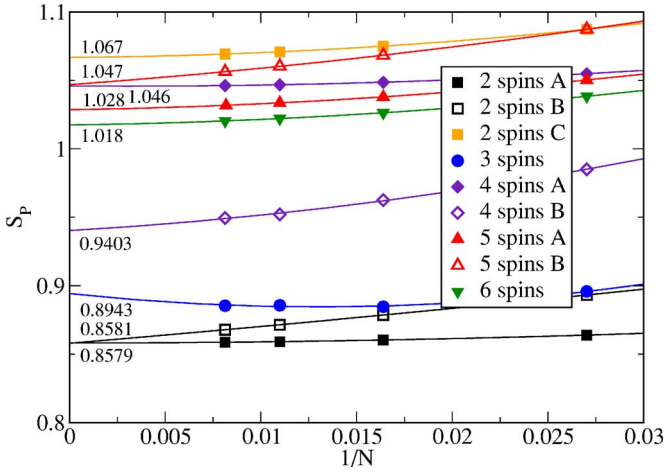

FIG. 6. (Color online) Effective actions S_P of different exchange processes for the Wigner crystal with mass anisotropy and lattice anisotropy. Orientation A is along the x axis. Two-spin A is the exchange between the second-nearest neighbor, two-spin B is the exchange between the nearest neighbor, and C is the exchange between the third-nearest neighbor (see Fig. 1). The curves are fits of the form $\alpha_0+\frac{\alpha_1}{N}+\frac{\alpha_2}{N^2}$; the extrapolated value of the thermodynamic limits are marked in the figure.

fitting. The corresponding curves are plotted with dashed lines in Fig. 7. In the case of five-spin exchange type B plotted with a dashed curve in Fig. 7, although four data points fall on a single fitting curve, this curve extrapolates to a negative value at $N=\infty$. All of these anomalies indicate that the algorithm for A_P, which involves a large determinant in each iteration, is not accurate enough for large anisotropic systems. We can estimate the error of this calculation from the difference between two three-particle exchange processes

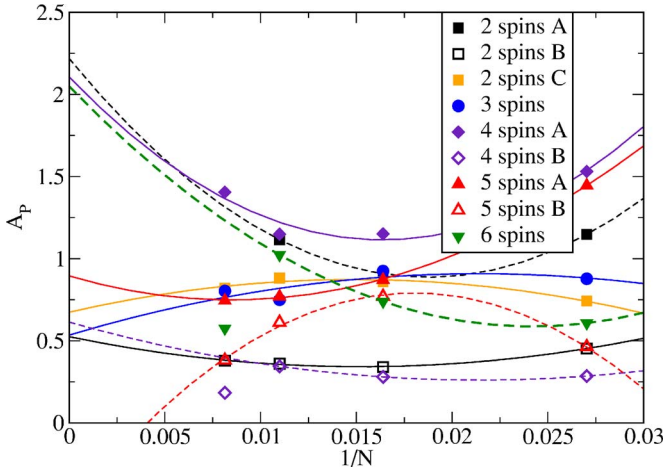

FIG. 7. (Color online) Numerical prefactors A_P of different exchange processes for the Wigner crystal with mass anisotropy and lattice anisotropy; orientation A is along the x axis. Two-spin A is the exchange between second-nearest-neighbor, two-spin B is the exchange between the nearest neighbor, and C is the exchange, between the third-nearest neighbor. The curves are fits of the form $\alpha_0+\frac{\alpha_1}{N}+\frac{\alpha_2}{N^2}$. See the text for the difference between the solid and the dashed lines.

with different orientations, which are related by a spatial inversion. These two processes should be equivalent as confirmed by the calculation of their S_P. They should also have the same A_P. However, our numerical results for their A_Ps are not exactly equal. For example, in the case of $N=91$, $(1/N\approx 0.011)$ in Fig. 7, the plotted value for a three-particle exchange is the average of 0.818 and 0.719, obtained from the two orientations of the exchange process. From this we deduce the relative error of A_P is about 10%. This broken inversion symmetry in A_P is probably due to the finite cluster size.

Comparing the above three cases, we see that the main difference between isotropic and anisotropic Wigner crystal is the dominant exchange process: the three-particle exchange dominates in the isotropic case, while the nearest-neighbor two-particle exchange dominates the anisotropic cases. These two processes have different signs in the Thouless Hamiltonian Eq. (1). We expect this will give rise to different magnetic ground states of the Wigner crystal and affect its properties at very low temperatures. This is explored in the next section.

III. 16-SITE CLUSTER CALCULATION

A. Ground-state phase diagram

The two-spin exchanges contribute to antiferromagnetic couplings in the Thouless Hamiltonian Eq. (1), while the three-spin exchanges contribute to ferromagnetic couplings. To find the ground state of the Thouless Hamiltonian for different values of the exchange frequencies, we diagonalize a small cluster containing 16 (4 by 4) spins with coupling J_{2A}, J_{2B}, J_3, and $J_{4A,B}$ (see Fig. 1). We ignore J_{2C} because as can be seen from Fig. 6, its effective action is too large to be of consequence at large r_s. A similar calculation was previously done for the exchange Hamiltonian of ^{3}He by Cross and Bhatt.[7] We exploit different symmetries in our system—discrete translational symmetry, inversion symmetry, and spin-rotation symmetry. However, there is no lattice rotation symmetry as compared to the bcc ^{3}He case.[7] We first generate a complete set of orthogonal basis states that simultaneously diagonalize all the commuting symmetry operators. Thus, the Hamiltonian is block diagonalized in each subspace labeled by total spin S, total spin in z direction S_z, and two Bloch wave vectors k_x and k_y. The Hamiltonian matrix in each subspace can be generated and diagonalized with little effort, since the dimensions of the subspaces are much smaller than 2.[16] In our case, the largest size was 238.

Figure 8 shows the result of the diagonalization for a Hamiltonian having J_{2A}, J_{2B}, and J_3, but not J_4. Here J_{2B} and J_3 are measured in units of J_{2A}. We found that the ground state jumps from maximal spin $S=8$ to a minimal spin $S=0$ state, suggesting a clear, first-order phase transition from ferromagnetic ground state to antiferromagnetic ground state along a curve in the $J_{2B}-J_3$ plane. The strong first-order transition suggests that the cluster calculation should be reliable. The general trend in this figure indicates that the ferromagnetic coupling J_3 has to increase beyond a critical value between J_{2B} and J_{2A} to make the ground state ferromagnetic. The phase diagram given by the ground-state con-

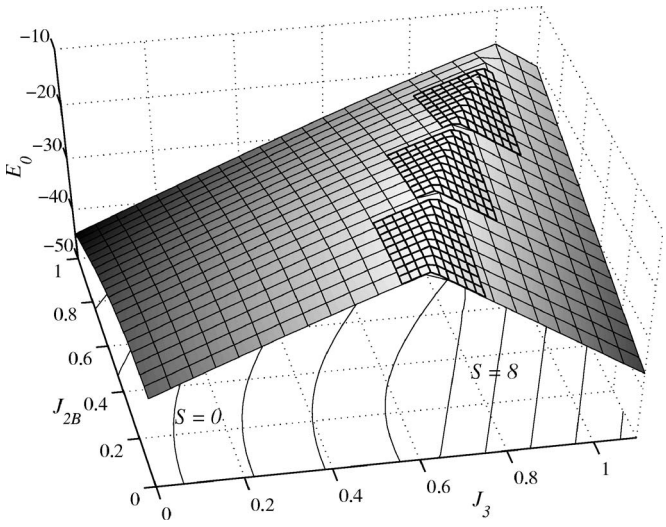

FIG. 8. Ground-state energy calculated by the direct diagonalization of 16 spin (4×4) clusters. $J_{2A}=1$. The planner region on the right results from the ferromagnetic ground state, whose energy is given by $16+16J_{2B}-48J_3$. This serves as a check of the accuracy of the numerical method. The curved region of the surface on the left corresponds to the energy of the antiferromagnetic ground state. Finer grids are used near the transition line to determine the phase boundary accurately.

figuration is shown in Fig. 9. We have studied the effect of a four-spin exchange by diagonalizing the Hamiltonian with a small J_{4A} and J_{4B}. Including J_{4A} and J_{4B} slightly decreases the ground-state energy of the antiferromagnetic phase, while slightly increasing the ground-state energy of the ferromagnetic phase. Consequently, we see a small shift of the phase boundary towards higher J_3, as indicated by the dashed line in Fig. 9. For small clusters, these effects are too small to qualitatively change the phase diagram.

In Fig. 9 we also mark the positions (J_{2B},J_3) for the ground state of the anisotropic Wigner crystal at various densities. The exchange frequencies are evaluated with the effective actions and prefactors obtained in Sec. II C. They appear to be in the antiferromagnetic phase in the low-density limit. The isotropic Wigner crystal corresponds to $J_{2B}=1$, $J_3>1$ in Fig. 9, which is in the ferromagnetic phase.

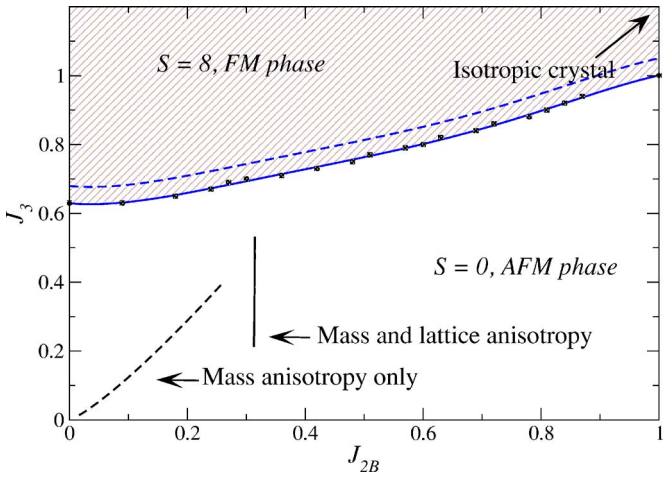

FIG. 9. (Color online) Phase diagram of the cluster. J_P is calculated using Eq. (4), with $40<r_s<1000$, and their trajectories are plotted in the antiferromagnetic phase of this figure. $r_s=1000$ is at the lower ends of these two short lines. The phase transition line is a polynomial curve fitting of the square data points, where the diagonalization shows to be near the edge of the transition.

B. Spin-spin correlation function

We evaluate the spin-spin correlation function of the ground state

$$C(\mathbf{r}_1-\mathbf{r}_2)=\langle\psi_0|\mathbf{S}_1\cdot\mathbf{S}_2|\psi_0\rangle, \tag{7}$$

with the ground-state wave function $|\psi_0\rangle$ obtained by diagonalizing the Hamiltonian. Here $\mathbf{r}_{1,2}=n\mathbf{a}_1+m\mathbf{a}_2$ are lattice vectors, where $\mathbf{a}_{1,2}$ are two basis vectors of the Bravias lattice. The Fourier transform of $C(\mathbf{r})$;

$$S(k_1,k_2)=\sum_{\mathbf{r}} e^{i\mathbf{k}\cdot\mathbf{r}}C(\mathbf{r}) \tag{8}$$

is calculated to illustrate the antiferromagnetic order of the ground state. A peak in $S(k_1,k_2)$ appears at (π,π) if the ground state has a 2D antiferromagnetic order. In the limit that both J_{2B} and J_3 are negligible, the system behaves as decoupled one-dimensional antiferromagnetic spin-1/2 chains. Let J_{2A} be along the direction of $\mathbf{a}_1$ and J_{2B} along $\mathbf{a}_2$. Then in this limit, $C(\mathbf{r})=C_n\delta_{m,0}$, while $S(k_1,k_2)$ turns out to be constant along k_2.

Table I lists the calculated $S(k_1,k_2)$ for selected values of exchange frequencies. The ground state wavefunctions were obtained from the Hamiltonian containing two-spin and three-spin exchange terms. For $J_{2B}=J_3=0.6$, $|S(\pi,\pi)|^2$ is one order of magnitude larger than the other terms, indicating a strong 2D antiferromagnetic order. For $J_{2B}=0.05$, $J_3=0$, $S(k_1,k_2)$ appears to be large at $k_1=\pi$, and has slight variation along k_2. We have verified numerically that for $J_{2B}=J_3=0$, $S(k_1,k_2)$ is independent of k_2. For $J_{2B}=0$, $J_3=0.6$, $|S(k_1,k_2)|^2$ behaves similarly to the previous case. However, $|S(\pi,\pi)|^2$ is equal to $|S(\pi,0)|^2$, instead of becoming the maximum

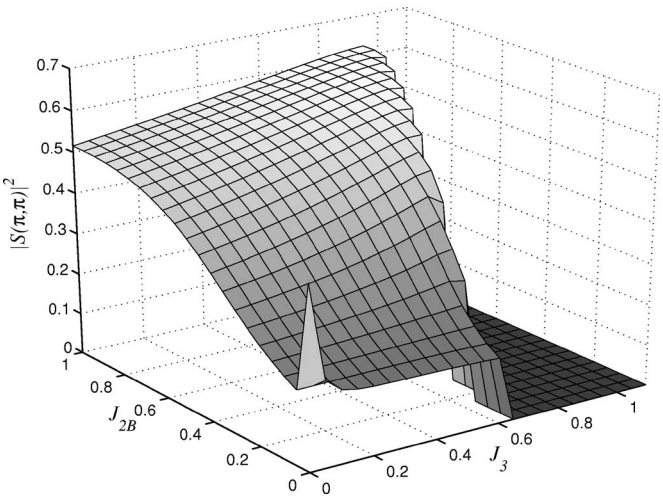

FIG. 10. $|S(\pi,\pi)|^2$ plotted as a function of J_{2B} and J_3 in the antiferromagnetic phase of exchange Hamiltonian with two-spin and three-spin exchange terms.

TABLE I. $|S(k_1,k_2)|^2$ of the ground state at selected exchange frequencies J_{2B} and J_3. J_{2A} is set to unity, while higher-order exchange terms are ignored.

	$k_2=0$	$k_2=\pi/2$	$k_2=\pi$	$k_2=3\pi/2$
	$J_{2B}=0.6$	$J_3=0.6$		
$k_1=0$	0.02387	0.03465	0.03800	0.03465
$k_1=\pi/2$	0.04760	0.04771	0.04760	0.04753
$k_1=\pi$	0.06163	0.07221	0.55808	0.07221
$k_1=3\pi/2$	0.04760	0.04753	0.04760	0.04771
	$J_{2B}=0.05$	$J_3=0$		
$k_1=0$	0.02387	0.02391	0.02395	0.02391
$k_1=\pi/2$	0.04734	0.04760	0.04786	0.04760
$k_1=\pi$	0.15416	0.16660	0.18248	0.16660
$k_1=3\pi/2$	0.04734	0.04760	0.04786	0.04760
	$J_{2B}=0$	$J_3=0.6$		
$k_1=0$	0.02388	0.02544	0.02647	0.02544
$k_1=\pi/2$	0.05630	0.05630	0.04340	0.04339
$k_1=\pi$	0.16006	0.1526	0.16006	0.15260
$k_1=3\pi/2$	0.05630	0.04340	0.04340	0.05630

value among the sixteen **k** points. This indicates that J_3 reduces the one-dimensional antiferromagnetic order along k_1, while it does not induce an antiferromagnetic correlation between neighboring chains, which J_{2B} obviously does.

Figure 10 shows $|S(\pi,\pi)|^2$ calculated from the ground state for (J_{2B},J_3) pairs in the antiferromagnetic phase. One can see that the peak at $J_{2B}=J_3=0$, corresponding to decoupled spin chains, is quickly reduced by a small J_3 or J_{2B}, while as J_{2B} increases, $|S(\pi,\pi)|^2$ gradually increases. At sufficiently large J_{2B}, J_3 also slightly contributes to this antiferromagnetic order parameter. This is because, in addition to the ferromagnetic coupling between nearest neighbors, three-spin exchange introduces ferromagnetic coupling between next-nearest neighbors on a square lattice, which is consistent with the antiferromagnetic order. So at the presence of a strong nearest-neighbor antiferromagnetic coupling due to two-spin exchanges, the effect of J_3 becomes a subtle balance between two competing tendencies. At the boundary of the antiferromagnetic phase, $S(\pi,\pi)$ does not vanish, which indicates a first-order phase transition in the ground state.

IV. CONCLUSION

We have presented a calculation of the exchange frequencies of multiparticle exchanges in two-dimensional Wigner crystals with anisotropy using the WKB method with an instanton approximation. The mass anisotropy that we have used, $m_x/m_y \approx 3$, is that of a Si(110) surface. The largest exchange frequency is found to be given by the two-particle exchange, rather than the three-spin exchange, which was found to dominate in the isotropic system at low densities. Furthermore, we have diagonalized the Thouless Hamiltonian on a 16-spin cluster, and found a transition from ferromagnetic ground state to antiferromagnetic ground state depending on the ratio of exchange frequencies. Combining these two results, we find that the ground state of the oblique Wigner crystal in an anisotropic system should have zero total spin, instead of being ferromagnetic. This change will alter the magnetic property of the Wigner crystal at low temperatures and corresponding physical pictures. In the extreme limit, when J_{2B} is very small, the Wigner crystal is a realization of antiferromagnetic spin-1/2 chains with weak ferromagnetic interchain coupling. Whether the ground state in the thermodynamic limit is antiferromagnetic, characterized by long-range antiferromagnetic order or a spin-liquid phase[8] or any other possibilities, is an open question. We expect to see a rich phase diagram depending on the electron density and effective mass anisotropy. Our approximations should be valid for anisotropic systems since the Wigner crystal exists at much lower densities in the anisotropic case than in the isotropic case. Nevertheless, it would be worthwhile to look at this problem using quantum Monte Carlo techniques,[2] especially in the vicinity of the melting density.

ACKNOWLEDGMENTS

We thank Z. Chen and K. Li of the Computer Science Department, Princeton University for generously sharing their computing facility with us. This research was supported by NSF Grant No. DMR-0213706. R.N.B. acknowledges the Aspen Center for Physics for hospitality during the final stage of completing this manuscript.

*Present address: Center for Nanophase Materials Science, Oak Ridge National Laboratory, P.O. Box 2008, Oak Ridge, Tennessee 37831-6493, USA, and Center for Simulational Physics, University of Georgia, Athens, Georgia 30602, USA.

[1] E. Wigner, Phys. Rev. **46**, 1002 (1934).
[2] B. Tanatar and D. M. Ceperley, Phys. Rev. B **39**, 5005 (1989).
[3] D. J. Thouless, Proc. Phys. Soc. London **86**, 893 (1965).
[4] Although the operator $\hat{P}$ in Eq. (1) exchanges spins rather than particle positions, the exchange interaction arises from the corresponding spatial exchange among identical particles. So each term in Eq. (1) is also considered to represent the exchange of particle positions. This becomes clear in Ref. 12, where the path integral of fermions is used to derive the exchange Hamiltonian, and the spatial degrees of freedom are integrated out.
[5] M. Roger, Phys. Rev. B **30**, 6432 (1984).
[6] M. Roger, J. M. Delrieu, and J. H. Hetherington, Rev. Mod. Phys. **55**, 1 (1983).
[7] M. C. Cross and R. N. Bhatt, J. Low Temp. Phys. **57**, 573 (1984); R. N. Bhatt and M. C. Cross, in *Proceedings of the 17th International Low Temperature Conference* (Elsevier, 1984), Vol. 17,

p. 283; M. C. Cross and R. N. Bhatt, Phys. Rev. B **33**, 7809 (1986).
[8] G. Misguich, B. Bernu, C. Lhuillier, and C. Waldtmann, Phys. Rev. Lett. **81**, 1098 (1998).
[9] M. Roger and J. M. Delrieu, Phys. Rev. B **39**, 2299 (1989).
[10] A. A. Katanin and A. P. Kampf, Phys. Rev. B **66**, 100403(R) (2002).
[11] B. Normand and A. M. Oleś, Phys. Rev. B **70**, 134407 (2004).
[12] K. Voelker and S. Chakravarty, Phys. Rev. B **64**, 235125 (2001).
[13] M. Muller, T. Vekua, and H.-J. Mikeska, Phys. Rev. B **66**, 134423 (2002).
[14] T. Sakai and Y. Hasegawa, Phys. Rev. B **60**, 48 (1999).
[15] A. Bühler, U. Löw, K. P. Schmidt, and G. S. Uhrig, Phys. Rev. B **67**, 134428 (2003).
[16] B. Bernu, L. Candido, and D. M. Ceperley, Phys. Rev. Lett. **86**, 870 (2001).
[17] G. Misguich, B. Bernu, C. Lhuillier, and C. Waldtmann, Phys. Rev. Lett. **81**, 1098 (1998).
[18] X. Wan and R. N. Bhatt, Phys. Rev. B **65**, 233209 (2002).
[19] A preliminary report of this work was presented at the International Conference on Ring Exchange and Correlated Fermions, 12–17 April 2004, Cargese, Corsica (France) [http://www-drecam.cea.fr/spec/cargese2004/programme.htm]; and also at the Annual APS March Meeting 2002 session Q18 [http://flux.aps.org/meetings/YR02/MAR02/baps/abs/S5780010.html]
[20] T. Ando, Rev. Mod. Phys. **54**, 437 (1982).